CrossMark

Adjustable, (super)hydrophobicity by e-beam deposition of nanostructured PTFE on textured silicon surfaces

A. F. Michels[1] · P. A. Soave[2] · J. Nardi[3] · P. L. G. Jardim[3] · S. R. Teixeira[3,4] ·
D. E. Weibel[3,5] · F. Horowitz[3,4]

Abstract Polytetrafluoroethylene (PTFE)-like films, produced by electron beam (e-beam) deposition, have shown higher hydrophobicity than those deposited by RF sputtering under similar deposition rates. It was found that this results from both surface chemical composition and nano-roughness. X-ray photoelectron spectroscopy measurements revealed that larger moieties of CF_2 and CF_3 groups were present to reduce surface energy in the e-beam deposited films. RF sputtering led to a higher degree of PTFE target fragmentation producing a different perfluorinated film on the Si substrate. Scanning electron microscopy and atomic force microscopy measurements revealed a much larger rms roughness on the film surfaces produced by e-beam (25.13 nm, at 20 mA) than those by RF sputtering (2.42 nm, at 100 W), and allowed a broad power spectrum density analysis with determination of the κ_B wetting parameter. In addition, the e-beam deposited films presented a linear increase of contact angle with applied electron current in the range under study (5–20 mA). This allows easy water repellency adjustment, up to $159 \pm 2°$.

For a superhydrophobic state with self-cleaning, a micro-pyramid structure was wet etched on the Si wafer, followed by PTFE deposition, and a very low contact angle ($163 \pm 2°$) and hysteresis was attained ($<3°$). These first results indicate that e-beam PTFE deposition with adjustable hydrophobicity may become a useful technique for integrated production with present Si microelectronics technology and for Si solar cells.

Introduction

For over a decade, several methods to obtain superhydrophobic surfaces have been developed due to great industrial interest in reducing flow resistance and fluidic drag [1], in repairable superomniphobic surfaces [2], in applications such as optical antireflection [3], corrosion protection [4], liquid transportation [5], biochemical separation [6], antibiofouling paints for boats, production of food packaging, inhibition of ice or snow adhesion [7, 8], and self-cleaning surface properties [9]. Although easy-dewetting surfaces can be obtained in flat/smooth surfaces even with low contact angle [10], superhydrophobic surfaces with self-cleaning properties are usually characterized by exhibiting a very high Contact Angle (CA) and low Contact Angular Hysteresis [11].

The hydrophobic properties of these surfaces depend on their chemistry and roughness [12]. In order to increase surface roughness, there are two possibilities: the first one is thorough its generation on the substrate, such as by plasma etching [13], chemical etching [14] or embossing [15]; the second is thorough incorporation of a coating on the substrate, such as by electrospinning [16–18], chemical vapor deposition [19–23], lithography [24, 25], dip coating [26, 27], anodic aluminum oxide [9, 28], sol–gel processing

✉ A. F. Michels
  alexandrefassinimichels@gmail.com

1 Universidade de Caxias do Sul, CP 1352, Caxias do Sul, RS CEP 95001-970, Brazil

2 Centro Federal de Educação Tecnológica de Minas Gerais, Araxá, MG CEP 38.180.510, Brazil

3 Programa de Pós-graduação em Ciência dos Materiais, Universidade Federal do Rio Grande do Sul, CP 15003, Porto Alegre, RS CEP 91501-970, Brazil

4 Instituto de Física, Universidade Federal do Rio Grande do Sul, CP 15051, Porto Alegre, RS CEP 91501-970, Brazil

5 Instituto de Química, Universidade Federal do Rio Grande do Sul, CP 15003, Porto Alegre, RS CEP 91501-970, Brazil

[29, 30] or physical vapor deposition (PVD) [15, 31]. Hierarchical structures, i.e., with micro- and nanostructure, have been reported for stability of the superhydrophobic condition [24].

The nanostructure allows the surface to sustain the highest pressure in nature, so as to maintain a robust Cassie state [32, 33]. At the same time, the microstructure significantly reduces the contact area, thereby largely removing adhesion between solid and fluid at the microscopic level [34]. On the other hand, tuning the surfaces in terms of low surface energy is favorable to super hydrophobic surfaces. In this context, a variety of coatings, such as siloxanes [35], fluoroalkylsilane [36], fluoroalkylphosphate [37], and polytetrafluoroethylene (PTFE) [38], have been used.

Many methods to obtain nanostructure and reduce the surface free energy are not easily scaled up, as they request very stringent conditions of preparation and are often obtained at high cost. In this sense, PTFE deposition by PVD methods is a good choice to provide nanostructure and reduce the surface free energy.

Previous reports are present in the literature on the properties of PTFE-sputtered films [39–41]. Particularly regarding chemical composition, wettability, and morphology, RF-sputtered PTFE coatings were grown under several bias voltages and gas compositions on silicon wafers [42, 43]. Thermally evaporated PTFE films have also been reported on several substrates, such as Aluminum [9], glass [44] intermetallic oxide alloys [45], micro- and nano-crystalline diamond-like carbon [46, 47] to promote low surface energy and surface nano-roughness. High-energy electron irradiation was used for the chemical modification of bulk PTFE [48–52].

Comparison of film structures and properties obtained by electron beam (e-beam) and by RF sputtering deposition of several materials has been reported [53–56], but not of PTFE, whose deposition by e-beam was not previously attempted to our best knowledge.

In this work, we report that PTFE deposited by e-beam, in one step, can significantly improve the hydrophobicity of a flat surface, by simultaneous incorporation of low surface energy and nanostructure. After a comparative study of the refractive index, hydrophobicity, surface chemistry, and nanostructure of PTFE-like coatings deposited by e-beam and by RF Sputtering, we pursue superhydrophobic behavior on a Si substrate.

Experimental

Materials

Silicon Prime (100) wafers were supplied by Wacker Chemitronic, polished on one side and doped as p-type.

These were sliced into rectangular, flat Si substrates ($25 \times 25 \times 0.6$ mm^3), which were cleaned in a piranha solution (H_2SO_4:H_2O_2 at 4:1) for 10 min at 120° C. After that, the Si substrates were rinsed in deionized water and then immersed in ammonium hydroxide solution (NH_4OH:H_2O_2:H_2O 1:1:4) for 10 min at 70–80 °C, followed by rinsing with copious amounts of deionized water and drying under nitrogen flow.

Polytetrafluoroethylene (PTFE) from Dupont was cleaned by ultrasound in isopropyl alcohol before deposition by physical vapor deposition (PVD), RF sputtering and e-beam, methods. Ethanol (98.5 %), H_2SO_4 (98 %), H_2O_2 (98.5 %), and NH_4OH (98 %) were supplied by Nuclear Brazil.

Physical vapor deposition methods

Electron beam bombardment (e-beam)

Teflon-like films were deposited by e-beam, using a PTFE target, on silicon substrates by a 3 kW Thermionics RCR0304-BD Electron Beam source. The e-beam system was pre-programmed to operate at a base pressure of about 4.0×10^{-6} Torr and work pressure of about 2.4×10^{-4} Torr. During deposition, the substrates remained fixed on a rotary sample system, at a distance of 40 cm from the target.

RF magnetron sputtering

Radio Frequency, Magnetron Plasma Sputtering of PTFE was carried out with a Leybold Univex 450B Sputtering System, using Ar sputtering gas plasma on a PTFE 7.5 cm diameter target, under RF (13.56 MHz) power. The system was pre-programmed to operate at a base pressure of about 4.0×10^{-6} Torr and work pressure of about 1.0×10^{-4} Torr. During the evaporation process, the samples were fixed on a rotary sample system at a distance of 15 cm from the PTFE target.

Chemical etching

1 % wt of KOH in water solution was used to etch the Silicon surface, which was left for 40 min in the solution at 80 °C. Pyramidal structures were formed, following the (1, 1, 1) Si cleavage plane.

Deposition rates

Film thicknesses and deposition rates were monitored, in real time, by a quartz crystal microbalance during both PVD processes. Comparable deposition rates were established, with regard to later comparison of the resulting films, as shown in Table 1.

Table 1 PVD deposition parameters during PTFE-like film production

PVD method	Power (W) or current (mA)	Deposition rate (nm/s)
RF sputtering	100	0.2
RF sputtering	150	0.3
RF sputtering	200	0.4
e-beam	5	0.2
e-beam	10	0.3
e-beam	20	0.4

Surface characterization

Scanning electron microscopy (SEM) and atomic force microscopy (AFM)

The morphology of the PTFE nanostructure was imaged by scanning electron microscopy (JEOL JSM 6060), using an electron acceleration of 15 kV, and by Atomic Force Microscopy (Dimension 3100 DIVM Group).

Surface Roughness and the Wetting Parameter κ_B, that relates wetting with surface topography [57–60], were evaluated using the PSD (Power Spectral Density) analysis.

X-ray photoelectron spectroscopy (XPS)

XPS spectra were obtained in a conventional electron spectrometer (Omicron) equipped with a high performance hemispherical energy analyzer, with a seven-channeltron detector and using Al Kα radiation as the excitation source. Surveys of spectra were recorded, with pass energy of 50 eV, whereas selected atomic signals were acquired with 10 eV of pass energy. In the spectra, the position of the C–C/C–H was specified and other peaks of different carbon environments were fixed, relative to this peak, set at 285.0 eV. The C 1 s envelope was analyzed and peak-fitted after the subtraction of a Shirley background, using Gaussian-Lorenzian peak shapes, obtained from the Casa XPS software package. Sputtering of Si substrates was carried out with a standard ion gun, using Ar ions as primary particles.

Contact angle measurement

Water contact angle was measured by the dynamic sessile drop method using a Krüss DS-30 goniometer. Droplets of deionized water were placed, with a motor-driven syringe, onto the sample surface. Each equilibrium contact angle was determined from a tangent line, appropriately positioned on the contour of the droplet with respect to the surface plane. The advancing and receding contact angles were measured on both sides of the drop for each sample.

The reported values are an average of more than 20 measurements, performed on at least three different locations of each sample surface, using a computer-controlled device (provided by Krüss).

Refractive index measurement

Thickness and refractive index of PTFE-like films were measured with the Spectroscopic Ellipsometer SOPRA GES-5E, which uses one rotating polarizer, one fixed analyzer and the Hadamard transform method. All measurements were performed at six different micro-spots on the sample, at a light beam angle of incidence of 68° and in the wavelength range of 350–750 nm.

Results and discussion

Figure 1 shows a comparative summary of the PTFE-like film properties, deposited on polished Si (100) substrates, by RF Sputtering and by e-beam. Contact angles and
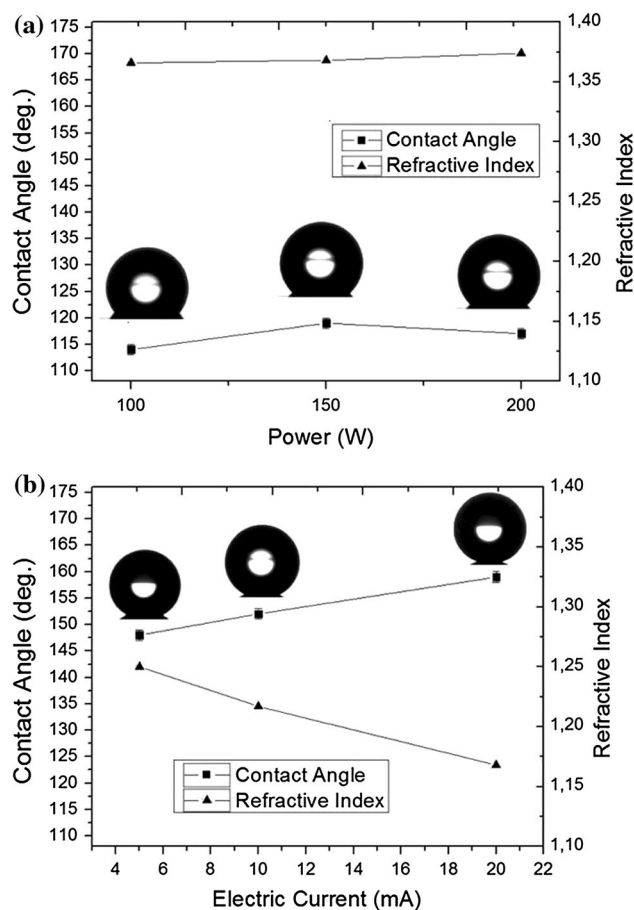
Fig. 1 Contact Angle and Refractive Index at 633 nm of PTFE-like films deposited on polished Si flat substrates by: **a** RF Sputtering at different Ar ion-beam energies, and **b** e-beam at different currents. Lines were drawn as an aid to the eye

Table 2 Properties of PTFE-like films on Si, deposited by RF sputtering and e-beam processes

PVD method	Contact angle (uncertainty: ± 2°)	Thickness (nm)	Refractive index
RF sputtering (100 W)	114	192	1.366
RF sputtering (150 W)	119	224	1.368
RF sputtering (200 W)	117	204	1.374
e-beam (5 mA)	152	74	1.250
e-beam (10 mA)	154	78	1.217
ce-beam (20 mA)	158	70	1.168

Hysteresis could not be measured because water drops did not move even with samples in a vertical position. In one run, even with sweeping, e-beam film thicknesses are smaller than those produced by rf sputtering due to higher consumption of deposition material where the e-beam energy was focused

refractive indices are shown, in Fig. 1a, for films deposited by RF argon plasma sputtering at three different powers (100, 150, and 200 W) and, in Fig. 1b, for films deposited by e-beam at three different currents (5, 10, and 20 mA).

Comparatively, as shown in Fig. 1 and Table 2, PTFE-like films deposited by RF Sputtering (Fig. 1a), present higher refractive indices than those obtained by e-beam (Fig. 1b). The refractive index of the RF-Sputtered films increased with deposition power (Fig. 1a) as expected, since higher Ar plasma energies promote molecular mobility during deposition, and thus higher film packing densities. Also sputtered molecules arrive at random angles on a near substrate, whereas a more collimated molecular flux arrives at longer distances during e-beam deposition. In this case, larger voids and thus smaller refractive indices can be produced, as shown in Fig. 1b and Table 2.

As reported in the literature, the contact angle of PTFE-like films, deposited by RF Sputtering, depends on Ar ion-beam energy [40, 41]. Basically, when large moieties of CF_2 and CF_3 groups are generated, the surface energy is reduced and thus the contact angle increases. Also the contact angle of PTFE-like films, obtained by e-beam (Fig. 1b and Table 2), increases with electron beam current.

Additionally, PTFE-like films obtained by e-beam can present higher contact angles than those obtained by RF Sputtering (see Fig. 1 and Table 2). These results can be originated from two factors: (1) the distinct surface chemical compositions of the treated samples, and (2) their different roughnesses, due to the presence of nanostructure.

XPS and SEM measurements were carried out to study in detail the surface chemical composition and morphology of both PVD methods. Figure 2 shows the C 1 s spectra of the PTFE-like films obtained by e-beam and by RF Sputtering. Both PVD methods produced a very different surface chemical composition of the prepared coatings. The C 1 s envelope of the e-beam method resembles a PTFE-like film [61], but with a value of the high-energy peak moved to even higher energies than a typical $–CF_2–$ signal in pure
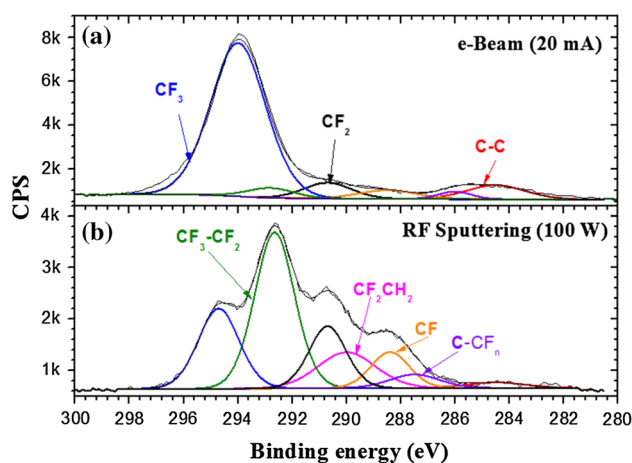
Fig. 2 XPS wide scan spectra of PTFE-like films deposited by: **a** e-beam with current of 20 mA and **b** RF Sputtering with power of 100 W

PTFE (292.53 eV). Therefore, the C 1 s signal position of 294.0 eV (Fig. 2a) can be assigned to a $–CF_3$ functionality [15, 42, 43, 62]. On the contrary, RF Sputtering led to a high degree of PTFE target fragmentation and recombination of the desorbed species on the surface of the Si substrate. Several C 1 s fluorinated chemical environments overlap in the deconvolution as shown in Fig. 2b. Oxidized functionalities, such as C=O or COO, can be included in the fittings as presented in Fig. 2b due to overlapping in binding energies. Partial oxidation of the surface was not observed in the XPS survey spectrum and therefore the contribution of functionalities such as C=O or COO can be ruled out. The larger moieties of CF_3 groups showed in Fig. 2a, as compared to Fig. 2b (RF Sputtering), may explain the higher contact angle of the films deposited by e-beam, since higher fluorine concentration at the surface given by the $-CF_3$ group would decrease even more the surface free energy compared to the RF Sputtering coating.

The second factor that contributed to higher contact angles from the e-beam deposited films, compared to those

(a)

(b)

(c)
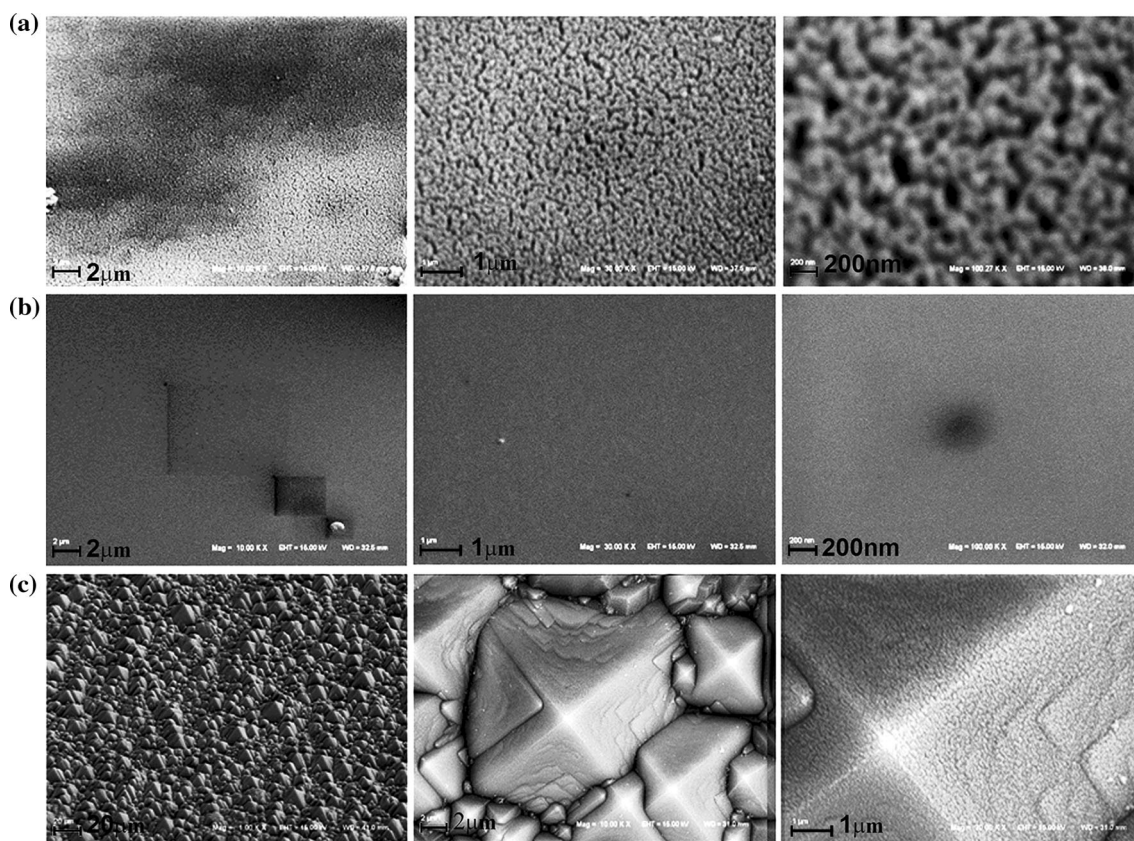
Fig. 3 SEM images of PTFE-like films deposited by: **a** e-beam on flat Si with current of 20 mA, **b** RF Sputtering on flat Si with power of 100 W and **c** e-beam on etched Si with current of 20 mA

from the RF-sputtered films, is the higher roughness of the former, which is evident in SEM Fig. 3 and AFM Fig. 3.

From the different AFM scan areas, the isotropic PSD functions can be combined into a single PSD function [60, 63] that contains the spectral representation of the morphology in a wide spectral range, as shown in Fig. 5. Here the PSD function related with the e-beam deposited films presents a peak around 10 μm^{-1}. This peak represents the micro- and nanostructure, with dimensions between 65 and 120 nm, presented in Fig. 4a.

From the PSD functions related to the e-beam and sputtering processes in Fig. 5, roughnesses and wetting parameters, whose values correspond to the areas below the PSD functions, can be calculated directly [57–60] and are shown in Table 3.

The sub-micrometer roughness produced by the e-beam, shown in Table 3, contributes to increasing the contact angle to values higher than those obtained by RF Sputtering. According to the necessary criterion for superhydrophobicity, $\kappa_B > 0.4$ [58, 60], the κ_B value for the e-beam deposition is close to the threshold for the superhydrophobic state. Also, the κ_B value for RF Sputtering in Table 3 explains why by this method a superhydrophobic

state could not be obtained, even with the existence of a fluorinated coating (see Fig. 2b).

Due to the two major factors, low surface energy and high roughness, PTFE-like films deposited by e-beam showed a superhydrophobic static behavior. Good adhesion of all the PTFE-like films on the Si (100) surfaces was verified by the Scotch tape test. However, their Contact Angular Hysteresis was high and thus full superhydrophobicity was not achieved. For this, before PTFE deposition, the Silicon substrate was subjected to chemical etching.

The resulting micro-pyramidal structures, shown in Fig. 3c, with the PTFE-like coating nanostructure, lead to a high contact angle ($163 \pm 2°$) and very small hysteresis ($<3°$), unlike those coated by RF sputtering ($154 \pm 2°$ and $40°$, respectively), which demonstrate that a full superhydrophobic state can be achieved by e-beam deposition of PTFE on silicon.

The Thermionics e-beam system presents a maximum power of 3KW, whereas the RF sputtering unit can reach a voltage of 3 kV. Since also the Ar+ mass is five orders of magnitude larger than that of the electron, the former presents a much larger momentum than the latter. Electron
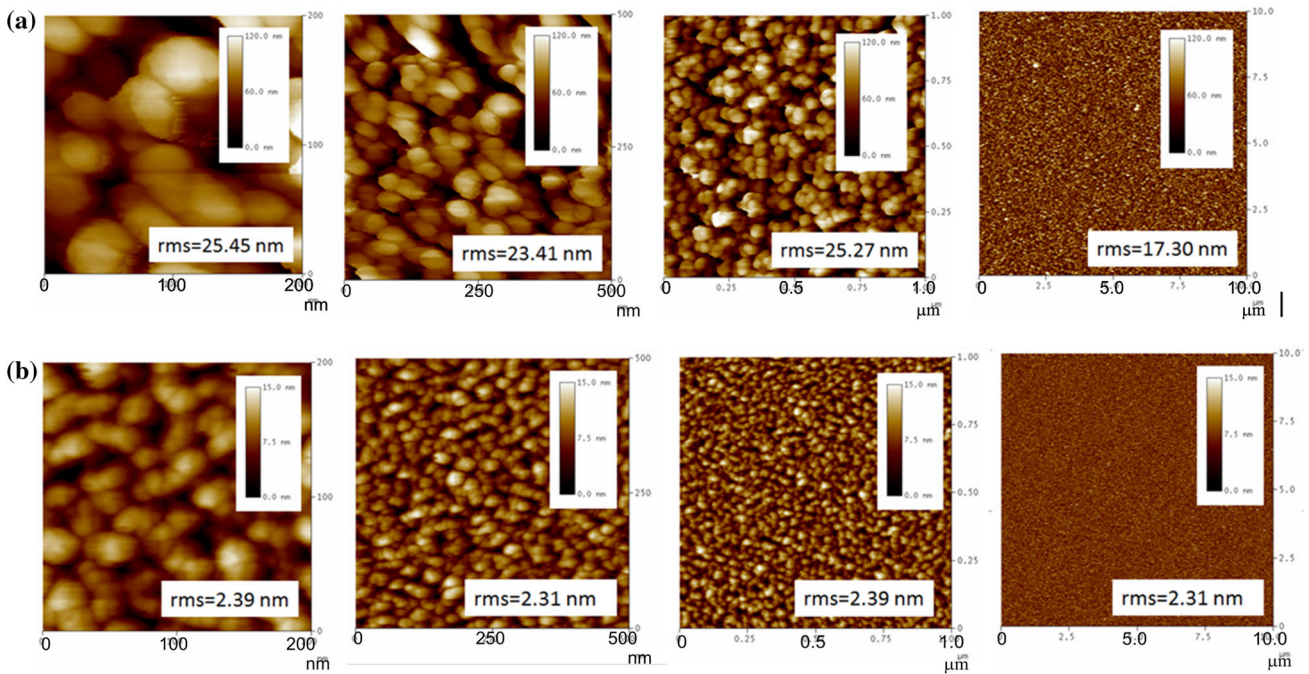
Fig. 4 AFM topography with 200-20,000 nm Scan Range area windows square side, where Root Mean Square (rms) roughnesses are shown for PTFE-like films deposited by: **a** e-beam with current of 20 mA and **b** RF Sputtering with power of 100 W
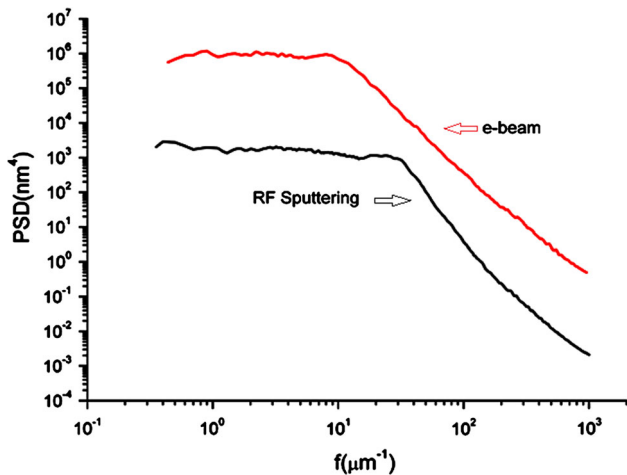
Fig. 5 PSD functions in a wide frequency range for PTFE-like films deposited by: (*red*) e-beam with current of 20 mA and (*black*) RF Sputtering with a power of 100 W (Color figure online)

bombardment is essentially a thermal process, whereas momentum transfer dominates in ion bombardment.

This implies that sputtering leads to a higher degree of PTFE target fragmentation and recombination of the desorbed species on the Si surface, as observed by XPS in Fig. 2, and also that the higher Ar plasma momenta promote molecular mobility during deposition, and thus higher film packing densities, resulting in higher refractive indices (Fig. 1; Table 2) and smaller roughnesses, as shown by SEM (Fig. 3) and by AFM (Fig. 4), as well as (via PSD, Fig. 5) in a smaller κ_B Wetting Parameter (Table 3).

Conclusions

A comparative study between PTFE-like coatings deposited by e-beam and by RF Sputtering, under similar deposition rates on flat Silicon substrates, was presented, based on SEM, XPS, Sessile drop, and Ellipsometric measurements. As discussed, Sputtering produces higher film packing densities, and thus higher refractive indices, with lower roughnesses. These, combined with the larger moieties of CF_2 and CF_3 groups that decrease surface free energy on the e-beam deposited films, result in higher contact angles, which can be linearly adjusted with applied current in the studied range (5–20 mA), up to 159 + 2°, although still with high hysteresis. Further micro-

Table 3 Roughness and κ_B wetting parameter obtained from the PSD functions of PTFE-like films

PVD method	Roughness (nm)	κ_B Wetting parameter
E-beam (20 mA)	25.13	0.36
RF sputtering (100 W)	2.42	0.05

structuring of the pre-coated Si surface by chemical etching allows an even higher contact angle (165 + 2°) with very low hysteresis (<3°). These first results indicate that one-step e-beam deposition is a promising production tool with present Si microelectronics technology, such as for digital microfluidic or lab-on-a-chip devices and for Si solar cells.

References

1. Gnanappa AK et al (2011) Contact line dynamics of a superhydrophobic surface: application for immersion lithography. Microfluid Nanofluidics 10:1351–1357
2. Rangel TC et al (2015) Superomniphobic and easily repairable coatings on copper substrates based on simple immersion or spray processes. Langmuir. doi:10.1021/acs.langmuir.5b00193
3. Kiraly B, Yang S, Huang TJ (2013) Multifunctional porous silicon nanopillar arrays: antireflection, superhydrophobicity, photoluminescence, and surface-enhanced Raman scattering. Nanotechnology 24:245704–245713
4. Ishizaki T, Masuda Y, Sakamoto M (2011) Corrosion resistance and durability of superhydrophobic surface formed on magnesium alloy coated with nanostructured cerium oxide film and fluoroalkylsilane molecules in corrosive nacl aqueous solution. Langmuir 27:4780–4788
5. Cho WK, Choi IS (2008) Fabrication of hairy polymeric films inspired by geckos: wetting and high adhesion properties. Adv Funct Mater 18:1089–1096
6. Menini R, Farzaneh M (2009) Elaboration of Al2O3/PTFE ice-phobic coatings for protecting aluminum surfaces. Surf Coat Technol 203:1941–1946
7. Nakajima A, Hashimoto K, Watanabe T (2001) Recent studies on super-hydrophobic films. Monatsh Chem 132:31–41
8. Sarkar DK, Farzaneh M (2009) Superhydrophobic coatings with reduced ice adhesion. J Adhes Sci Technol 23:1215–1237
9. Weibel DE et al (2010) Adjustable hydrophobicity of Al substrates by chemical surface functionalization of nano/microstructures. J Phys Chem C 114:13219–13225
10. Masheder B et al (2013) Novel transparent zirconium-based hybrid material with multilayered nanostructures: studies of surface dewettability toward alkane liquids. ACS Appl Mater Inter 5:154–163
11. Celia E et al (2013) Recent advances in designing superhydrophobic surfaces. J Colloid Interface Sci 402:1–18
12. Cassie ABD, Baxte S (1944) Wettability of Porous Surfaces. Trans Faraday Soc 40:546–551
13. Long CJ, Schumacher JF, Brennan AB (2009) Potential for tuneable static and dynamic contact angle anisotropy on gradient microscale patterned topographies. Langmuir 25:12982–12989
14. Xiaocheng L et al (2009) Fabrication of silicon pyramid/nanowire binary structure with superhydrophobicity. Appl Surf Sci 255:7147–7152
15. Gong D et al (2015) Thermal stability of micro–nano structures and superhydrophobicity of polytetrafluoroethylene films formed by hot embossing via picosecond laser ablated template. Appl Surf Sci 331:437–443
16. Hardman SJ et al (2011) Electrospinning superhydrophobic fibers using surface segregating end-functionalized polymer additives. Macromolecules 44:6461–6470
17. Ding B et al (2008) Fabrication of a super-hydrophobic nanofibrous zinc oxide film surface by electrospinning. Thin Solid Films 516:2495–2501
18. Grignard B et al (2011) Electrospinning of a functional perfluorinated block copolymer as a powerful route for imparting superhydrophobicity and corrosion resistance to aluminum substrates. Langmuir 27:335–342
19. Lau KKS et al (2003) Superhydrophobic carbon nanotube forests. Nano Lett 3:1701–1705
20. Borras A, Barranco A, Gonzalez-Elipe AR (2008) Reversible superhydrophobic to superhydrophilic conversion of Ag@TiO2 composite nanofiber surfaces. Langmuir 24:8021–8026
21. Jung YC, Bhushan B (2009) mechanically durable carbon nanotube-composite hierarchical structures with superhydrophobicity, self-cleaning, and low-drag. ACS Nano 3:4155–4163
22. Journet C et al (2005) Contact angle measurements on superhydrophobic carbon nanotube forests: effect of fluid pressure. Europhys Lett 71:104–109
23. Balu B, Breedveld V, Hess DW (2008) Fabrication of "roll-off" and "sticky" superhydrophobic cellulose surfaces via plasma processing. Langmuir 24:4785–4790
24. Li Y et al (2010) Bioinspired silica surfaces with near-infrared improved transmittance and superhydrophobicity by colloidal lithography. Langmuir 26:9842–9847
25. Yang H et al (2011) Tailoring the wettability of patterned silicon surfaces with dual-scale pillars: from hydrophilicity to superhydrophobicity. Appl Surf Sci 257:7689–7692
26. Camargo KC et al (2012) Multi-scale structured, superhydrophobic and wide-angle, antireflective coating in the near-infrared region. Chem Commun 48:4992–4994
27. Gao L, He J (2013) A facile dip-coating approach based on three silica sols to fabrication of broadband antireflective superhydrophobic coatings. J Colloid Interface Sci 400:24–30
28. Shirtcliffe NJ et al (2004) Dual-scale roughness produces unusually water-repellent surfaces. Adv Mater 16:1929–1932
29. Mahadik SA (2010) Transparent Superhydrophobic silica coatings on glass by sol–gel method. Appl Surf Sci 257:333–339
30. Wu XD, Zheng LJ, Wu D (2005) Fabrication of superhydrophobic surfaces from microstructured ZnO-based surfaces via a wet-chemical route. Langmuir 21:2665–2667
31. Kulinich SA, Farzaneh (2009) Ice adhesion on super-hydrophobic surfaces. Appl Surf Sci 255:8153–8157
32. Cassie ABD (1948) Contact angles. Discus Faraday Soc 3:11–16
33. Cheng YT et al (2006) Effects of micro- and nano-structures on the self-cleaning behaviour of lotus leaves. Nanotechnology 17:1359–1362
34. Balani K et al (2009) The hydrophobicity of a lotus leaf: a nanomechanical and computational approach. Nanotechnology 20:305707–305715
35. Wang S et al (2011) Preparation of a durable superhydrophobic membrane by electrospinning poly (vinylidene fluoride) (PVDF) mixed with epoxy-siloxane modified SiO2 nanoparticles: a possible route to superhydrophobic surfaces with low water sliding angle and high water contact angle. J Colloid Interface Sci 359:380–388
36. Zhang L, Sun J (2010) Layer-by-layer codeposition of polyelectrolyte complexes and free polyelectrolytes for the fabrication of polymeric coatings. Macromolecules 43:2413–2420
37. Yang S et al (2011) Control of morphology and surface wettability of anodic niobium oxide micro cones formed in hot phosphate-glycerol electrolytes. Electrochim Acta 56:7446–7453

38. Camargo KC et al (2012) Visible and near infrared, wide-angle, anti-reflection coatings with self-cleaning on glass. Opt Mater Express 2:969–977

39. Bodasa DS, Mandalea AB, Gangala SA (2005) Deposition of PTFE thin films by RF plasma sputtering on (100) silicon substrates. Appl Surf Sci 245:202–207

40. Zhang Y et al (2002) Deposition of fluoropolymer films on Si (100) surfaces by Rf magnetron sputtering of poly(tetrafluoroethylene). Langmuir 18:6373–6380

41. Huang F et al (2007) Surface functionalization of silk fabric by PTFE sputter coating. J Mater Sci 42:8025–8028. doi:10.1007/s10853-007-1580-3

42. Yang GH, Zhang Y, Kang ET, Neoh KG (2003) Deposition of ultrathin fluoropolymer films on Si(100) and GaAs(100) surfaces by RF magnetron sputtering of poly(tetrafluoroethylene-co-hexafluoropropylene). J Phys Chem B 107:2780–2787

43. Henry F et al (2012) Synthesis of superhydrophobic PTFE-like thin films by self-nanostructuration in a hybrid plasma process. Surf Sci 606:1825–1829

44. Yao L, He Z (2014) Recent progress in antireflection and self-cleaning technology—from surface engineering to functional surfaces. Prog Mater Sci 61:94–143

45. Feil AF et al (2011) Micro and nano-texturization of intermetallic oxide alloys by a single anodization step: preparation of artificial self-cleaning surfaces. ACS Appl Mater Interfaces 3:3981–3987

46. Horowitz F et al (2013) Nano-microstructured, superhydrophobic, and infrared transparent polytetrafluoroethylene/diamond films. J Nanophoton 7:073596. doi:10.1117/1.JNP.7.073596

47. Brandão LEV et al (2013) Wettability of PTFE coated diamond films. Surf Coat Technol 232:384–388

48. Lappan U, Geissler U, Lunkwitz K (1999) Modification of polytetrafluoroethylene by electron beam irradiation in various atmospheres. Nucl Instrum Meth B 151:222–226

49. Dorschner H, Lappan U, Lunkwitz K (1998) Electron beam facility in polymer research: radiation induced functionalization of polytetrafluoroethylene. Nucl Instrum Meth B 139:495–501

50. Lunkwitz K, Lappan U, Lehmann D (2000) Modification of fluoropolymers by means of electron beam irradiation Radiat. Phys Chem 57:373–376

51. Lee EJ et al (2011) Surface morphology control of polymer films by electron irradiation and its application to superhydrophobic surfaces. ACS Appl Mater Interface 3:2988–2993

52. Lunkwitz K, Lappan U, Scheler U (2004) Modification of perfluorinated polymers by high-energy irradiation. J Fluorine Chem 125:863–873

53. Pradhan SK et al (2005) Deposition of CrN coatings by PVD methods for mechanical application. Surf Coat Technol 200:141–145

54. Porqueras I et al (2005) Characteristics of e-beam deposited electrochromic CeO2 thin films. Solid State Ionics 165:131–137

55. Ristau D et al (2005) Ultraviolet optical and microstructural properties of MgF_2 and LaF_3 coatings deposited by ion-beam sputtering and boat and electron-beam evaporation. Appl Opt 41:3196–3204

56. Cosnier V, Olivier M, Théret G, Andre B (2001) HfO_2-SiO_2 interface in PVD coatings. J Vac Sci Technol 19:2267–2271

57. Duparré A, Flemming M, Steinert J, Reihs K (2000) Optical coatings with enhanced roughness for superhydrophobic, low-scatter applications. Appl Opt 41:3294–3298

58. Flemming M, Coriand L, Duparré A (2009) A ultra-hydrophobicity through stochastic surface roughness. J Adhes Sci Technol 23:381–400

59. Coriand L, Mitterhuber M, Duparré A, Tünnermann (2011) A definition of roughness structures for superhydrophobic and hydrophilic optical coatings on glass. Appl Opt 50:257–263

60. Duparré A et al (2002) Surface characterization techniques for determining the root-mean-square roughness and power spectral densities of optical components. Appl Opt 41:154–171

61. Girardeaux C, Pireaux JJ (1996) Analysis of poly(tetrafluoroethylene) (PTFE) by XPS. Surf Sci Spectra 4:138–141

62. Schurmann U et al (2005) Controlled syntheses of Ag-polytetrafluoroethylene nanocomposite thin films by co-sputtering from two magnetron sources. Nanotechnology 16:1078–1082

63. Frré-Borrull J, Duparré A, Quesnel E (2001) Procedure to characterize microroughness of optical thin films: application to ion-beam-sputtered vacuum-ultraviolet coatings. Appl Opt 40:2190–2199